ACS OMEGA

Article

Cite This: ACS Omega 2019, 4, 13972−13980

http://pubs.acs.org/journal/acsodf

Performance and Stability Improvement of Layered NCM Lithium-Ion Batteries at High Voltage by a Microporous Al_2O_3 Sol−Gel Coating

Yingqiang Wu,[†] Mengliu Li,[†] Wandi Wahyudi,[†] Guan Sheng,[†] Xiaohe Miao,[§] Thomas D. Anthopoulos,[†] Kuo-Wei Huang,*[,†] Yangxing Li,*[,‡] and Zhiping Lai*[,†]

[†]Division of Physical Science and Engineering, King Abdullah University of Science and Technology (KAUST), Thuwal 23955-6900, Saudi Arabia

[‡]Watt Research Lab, Central Research Institute, Huawei Technologies Company Limited, Bantian, Longgang District, Shenzhen 518129, China

[§]Core Labs, King Abdullah University of Science and Technology (KAUST), Thuwal 23955-6900, Saudi Arabia

Supporting Information

ABSTRACT: A simple and low-cost polymer-aided sol−gel method was developed to prepare γ-Al_2O_3 protective layers for Li-$Ni_{0.6}Co_{0.2}Mn_{0.2}O_2$ (NCM622) cathode materials. The selected polyvinyl alcohol polymer additive not only facilitates the formation of a uniform and thin γ-Al_2O_3 layer on the irregular and rough cathode particle surface to protect it from corrosion but also serves as a pore-forming agent to generate micropores in the film after sintering to allow fast transport of lithium ions, which guaranteed the excellent and stable battery performance at high working voltage. Detailed studies in the full battery mode showed that the leached corrosion species from the cathode had a more profound harmful effect to the graphite anode, which seemed to be the dominating factor that caused the battery performance decay.

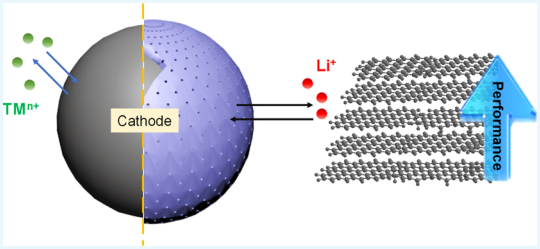

INTRODUCTION

Lithium-ion batteries (LIBs) have revolutionized the market of electronic power devices since their commercialization in 1991.[1−3] To pursue higher energy density LIBs, a high capacity cathode material is in great demand. One way to improve the energy capacity is to use Ni-rich layered lithium transition metal (TM) oxides ($LiNi_xCo_yMn_zO_2$, NCM_{xyz}), which can deliver up to 195 mA·h g^{-1} when the Ni content reaches 0.8.[4,5] Another strategy is to increase the charge cutoff voltage. For example, a capacity of 200 mA·h g^{-1} can be achieved for NCM622 under a charge cutoff voltage of 4.55 V (vs Li/Li^+).[6,7] However, both strategies can cause serious safety issues and quick performance decay. It is commonly believed that the cathode degradation is the predominant reason, where the highly reactive Ni^{4+} and Co^{4+} induce electrolyte decomposition and cathode oxygen loss, subsequently resulting in phase transformation from the layered structure (i.e., "O_3" phase) to the rock-salt structure and TM ion dissolution.[8−12] Another decay mechanism is attributed to the irreversible consumption of lithium ions for the solid electrolyte interface (SEI) formation on the anode (i.e., graphite), which is mainly caused by the deposition of dissolved TM ions from the NCM cathode on the surface of the anode.[13,14] This degradation becomes more serious when cycled at high voltage (4.5 V vs graphite) and high temperature, especially for the Ni-rich NCM whose phase transition occurs more easily. Thus, many efforts have been made to improve the surface structure stability of Ni-rich layered oxide cathodes via surface coating with various protection materials such as Al_2O_3,[15−17] TiO_2,[18−20] ZrO_2,[21−23] $AlPO_4$,[24−26] AlF_3,[27−29] and so forth. The general objective of these approaches is to prevent direct contact of the electrode from the electrolyte to reduce the potential parasitic side reactions at the cathode electrode/electrolyte interface. However, it is noted that all of these reported coatings have a dense structure, which inevitably impedes the transport of lithium ions and thus limits the performance improvement, particularly at a high voltage where the slow transport of lithium ions will cause serious concentration polarization. To increase the lithium-ion transport rate, one way is to reduce the layer thickness, but this requires expensive methods such as atomic layer deposition.[30−32] Thus, it is still a challenge to develop a practical approach to achieve a thin, uniform, and low-cost coating with good lithium-ion permeability. Moreover, most of these studies focused on the performance decay of the cathode, while the influence to the anode has not been fully studied, particularly at high voltage.

In this work, a polymer-aided sol−gel process is developed to prepare a microporous γ-Al_2O_3 protection layer on the NCM layered oxide cathodes (e.g., $LiNi_{0.6}Co_{0.2}Mn_{0.2}O_2$,

Received: June 10, 2019
Accepted: August 1, 2019
Published: August 19, 2019

DOI: 10.1021/acsomega.9b01706
ACS Omega 2019, 4, 13972−13980

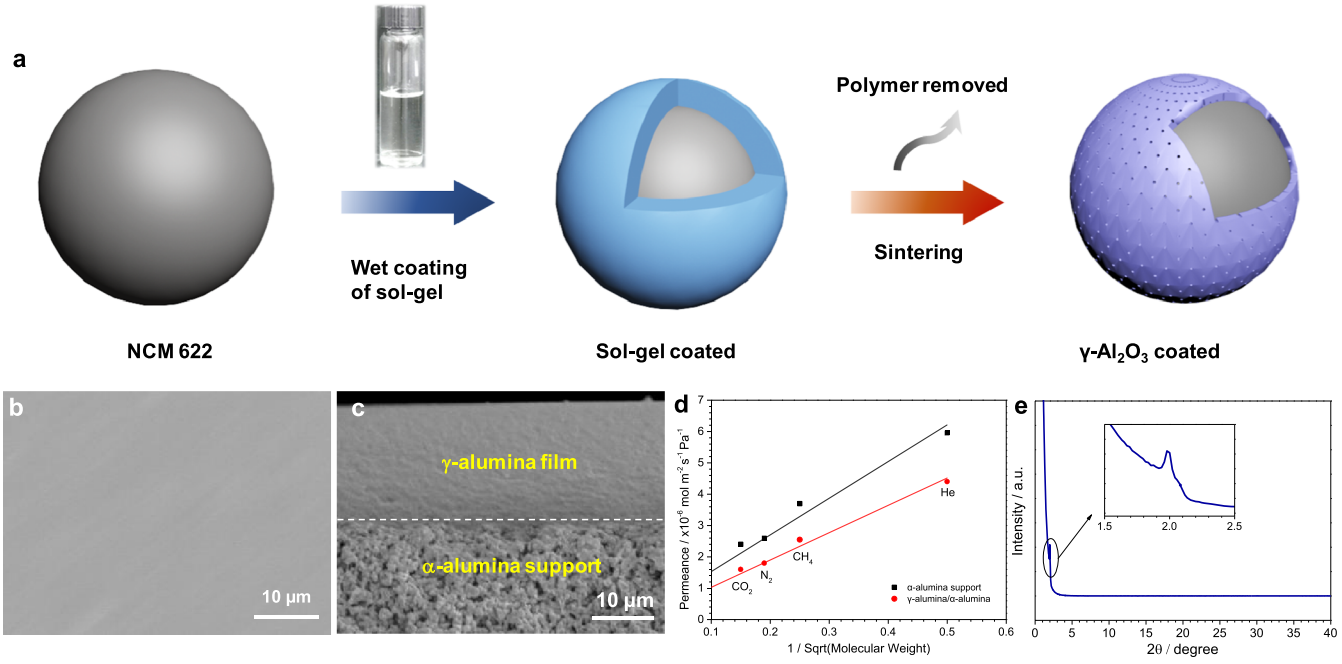

Figure 1. Features of the polymer/γ-Al_2O_3 coating. (a) Schematic illustration of the surface coating process on NCM622 particles. SEM images of (b) top view and (c) cross section for the polymer/γ-Al_2O_3 coating layer on the α-alumina substrate. (d) Relative gas permeation test for the polymer/γ-Al_2O_3 coating layer on the α-alumina substrate. (e) XRD pattern of the polymer/γ-Al_2O_3 film on a glass slide. The inset graph is the enlarged eclipse zone.

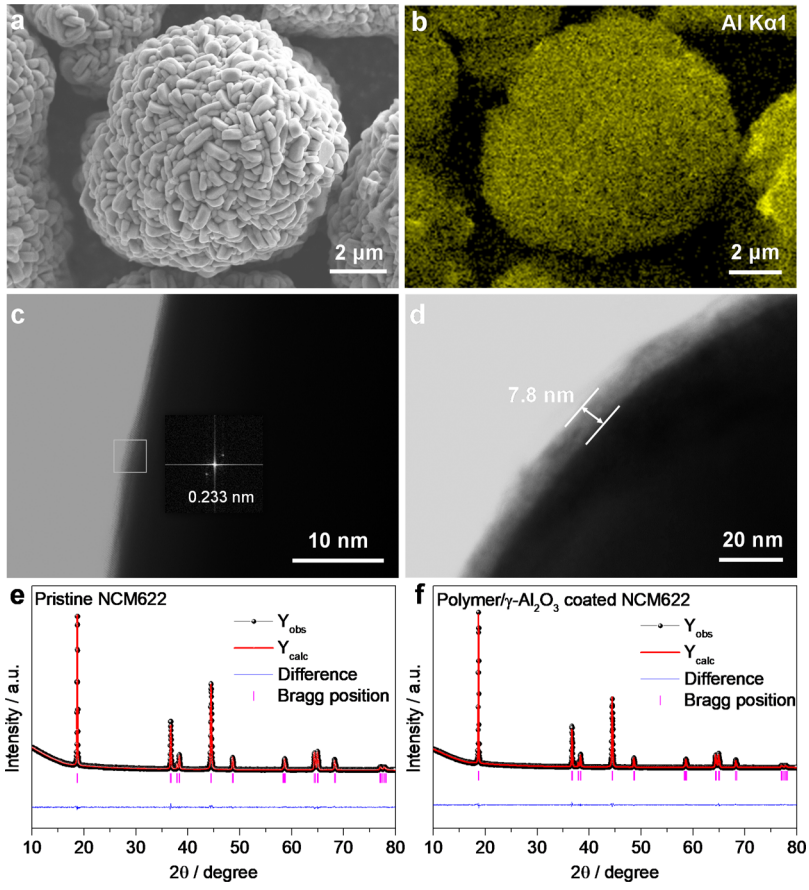

Figure 2. Materials characterization of the polymer/γ-Al_2O_3 coating. (a) SEM image and (b) corresponding EDX mapping of aluminum for a polymer/γ-Al_2O_3-coated NCM622 sample. TEM images of the (c) pristine NCM622 and (d) polymer/γ-Al_2O_3-coated NCM622 samples. XRD plots and the Rietveld refinement of the (e) pristine NCM622 and (f) polymer/γ-Al_2O_3-coated NCM622 samples.

DOI: 10.1021/acsomega.9b01706
ACS Omega 2019, 4, 13972−13980

Table 1. Cell Parameters, Cation Disorder, and Rietveld Refinement of the Electrode Materials before and after Coating

	a/Å	b/Å	c/Å	V/Å^3	Li/Ni disorder/%	R_{wp}/%
pristine NCM622	2.86947	14.23067	4.95934	101.4751	2.424	7.39
coated NCM622	2.86988	14.23293	4.95942	101.4143	2.448	7.17

pristine NCM622						polymer/γ-Al_2O_3-coated NCM622					
		position						position			
atom	site	x	y	z	Occ	atom	site	x	y	z	Occ
Li	3a	0	0	0	0.9758	Li	3a	0	0	0	0.9756
Ni		0	0	0	0.0242	Ni		0	0	0	0.0245
Li	3b	0	0	0.5	0.0242	Li	3b	0	0	0.5	0.0245
Ni		0	0	0.5	0.5760	Ni		0	0	0.5	0.5760
Co		0	0	0.5	0.2003	Co		0	0	0.5	0.2002
Mn		0	0	0.5	0.2000	Mn		0	0	0.5	0.2002
O	6c	0	0	0.2433	1.0001	O	6c	0	0	0.2427	1.0000

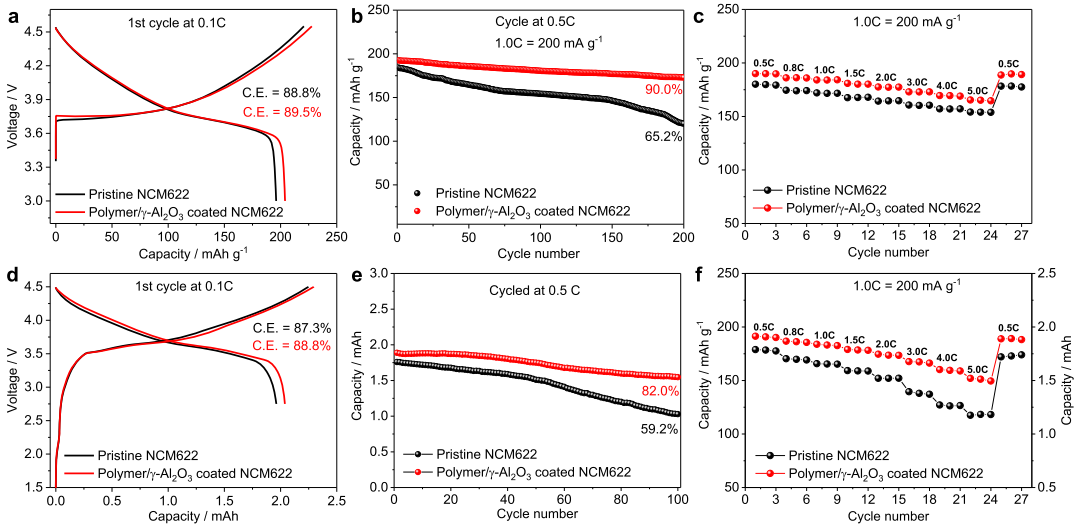

Figure 3. Comparative high-voltage performances of the half and full battery. Half-cell comparison of the (a) first cycle capacity and C.E. at 0.1 C, (b) cycling performance at 0.5 C, and (c) rate discharge capability of the batteries using the pristine and polymer/γ-Al_2O_3-coated NCM622 cathode, where the charge rate is 0.5 C. (d–f) Relative comparisons for full battery performance. 1 C = 200 mA g^{-1}.

NCM622). The selected polyvinyl alcohol (PVA) polymer can facilitate the film forming while leaving micropores in the film after sintering. This method could give rise to an ultrathin yet uniform and microporous coating layer on the irregular particle surface through a simple sol–gel coating process. The thickness of the coating layer is controlled less than 10 nm, benefiting from the excellent film-forming capability of the polymer/γ-Al_2O_3 sol–gel. The ultrathin and microporous γ-Al_2O_3 coating does not hinder the lithium diffusion process, while enhancing the NCM622 electrochemical performances at high voltage. The decay mechanism of the full battery using a graphite anode at 4.5 V is also studied. The results showed that the cycling degradation of the full battery with a pristine NCM622 cathode was mainly due to the irreversible consumption of lithium ions for SEI on the graphite anode, which was caused by the TM ions leached from the cathode. The ultrathin and uniform γ-Al_2O_3 coating could effectively suppress the dissolution of the TM ions and protect the graphite anode from their poison, thus guaranteeing the excellent and stable battery performance.

RESULTS AND DISCUSSION

The coating process for the NCM622 cathode material with the transparent polymer/γ-Al_2O_3 sol–gel is illustrated in Figure 1a. NCM622 particles were first soaked in a diluted polymer/γ-Al_2O_3 sol–gel for about 30 min, dried, and then calcined at 550 °C to remove the polymer while leaving the γ-Al_2O_3 coating layer with micropores. In order to demonstrate the microporous feature of the γ-Al_2O_3 coating layer, the prepared polymer/γ-Al_2O_3 sol–gel was coated with enough thickness on a porous α-Al_2O_3 substrate. The top-view and cross-sectional images showed that a smooth and continuous layer on top of the α-Al_2O_3 porous support was formed after calcination (Figure 1b,c). The layer is highly permeable, as illustrated by the gas permeation data in Figure 1d. The permeance of different gases has an inversely linear relationship with the square root of the molecular weight, indicating a Knudsen diffusion transport mechanism. The small-angle X-ray diffraction (XRD) of the coating layer displayed a peak at 2θ angle around 2.0° (Figures 1e and S1a), indicating that the film had a uniform porous structure with a pore size of around 3.6 nm. The Raman spectra of the coating layer (Figure S11) confirmed the γ-alumina phase. For comparison, Figure S1b,c shows the film made of pure sol without the PVA additive. It can be clearly observed that the top γ-Al_2O_3 layer was rougher and had thermally induced cracks. The layer also detached from the α-Al_2O_3 porous support, suggesting the poor adhesion properties of the pure sol. These results indicated

DOI: 10.1021/acsomega.9b01706
ACS Omega 2019, 4, 13972–13980

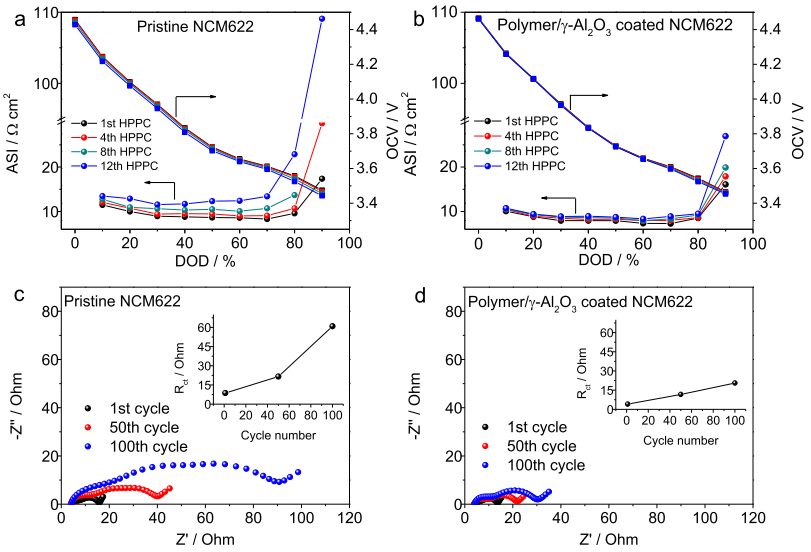

Figure 4. Kinetics and impedance comparison. Comparison of dc resistance measured by HPPC of (a) pristine NCM622 and (b) polymer/γ-Al_2O_3-coated NCM622 batteries. ac resistance measured by the EIS of (c) pristine NCM622 and (d) polymer/γ-Al_2O_3-coated NCM622 batteries.

the excellent film-forming capability and the good adhesion of the polymer/γ-Al_2O_3 sol−gel, which is crucial for giving rise to an ultrathin yet uniform and porous coating layer.

The scanning electron microscopy (SEM) image of the polymer/γ-Al_2O_3-coated NCM622 sample showed that there was no visible change to the morphology after calcination (Figure 2a). The energy-dispersive X-ray spectroscopy (EDX) analysis (Figure 2b) demonstrated an even distribution of aluminum, indicating a uniform coating of the γ-Al_2O_3 layer on the particle surface. Detailed inspection of the surface layer by transmission electron microscopy (TEM) (Figure 2c,d) revealed that the layer was around 7.8 nm on the particle surface, which was near to the theoretical value of 6.02 nm (calculation with the γ-Al_2O_3 equation of $L = m/\rho S$, where L is the thickness of the coating layer, m is the coating weight [1 wt %, inductively coupled plasma (ICP) analysis in Table S1), ρ is the density of γ-Al_2O_3 (3.8 g cm^{-3}), and S is the superficial area of NCM622 (0.437 m^2 g^{-1})], demonstrating the uniform coating layer. Further XRD analyses of the NCM622 materials before and after the coating are shown in Figure 2e,f. All diffraction peaks matched with the standard patterns of NCM622, but no signal from the Al_2O_3 coating layer was observed, which was presumably due to the ultrathin thickness.[30] Rietveld refinement of the XRD patterns revealed that the Li/Ni cation disorder for the coated and uncoated NCM622 framework were both around 2.4%, proving that the coating process did not affect the structure of the pristine NCM material (Table 1).

Figure 3a shows the initial capacities of the pristine and polymer/γ-Al_2O_3-coated NCM622 measured at high voltage (i.e., 4.55 V vs Li/Li^+) in half battery using lithium as the anode. The polymer/γ-Al_2O_3-coated NCM622 delivered a bit higher capacity compared to the pristine one (203.97 mA·h g^{-1} vs 196.07 mA·h g^{-1}), which could be ascribed to the γ-Al_2O_3 coating layer which improves the interface stability and the Coulombic efficiency (C.E., 89.8 vs 88.8%). The long-term cycling performance was also compared under 0.5 C (Figure 3b). The polymer/γ-Al_2O_3-coated NCM622 displayed excellent cycling stability and maintained a capacity retention of around 90% after 200 cycles under 4.55 V, which was 24.8% higher than that of the pristine sample. For comparison, NCM622 coated with pure Al_2O_3 sol without the PVA additive was also prepared similarly, and the initial capacity and long-term cycling performance are shown in Figure S2. Note that the initial C.E. increased to 89.1%, which also demonstrated a more stable interface of NCM622 after the Al_2O_3 coating. However, the cycled capacity decreased much faster compared to the coating sample with the PVA additive, and the capacity retention was only around 82% after 200 cycles, which could be due to the nonuniform, thick, and dense coating layer (Figure S1). While with the aid of PVA, a thin, uniform, and microporous coating layer was achieved (Figure 2), where the lithium ions diffused easily through the micropores in the coating layer with low interface impedance.[33] Thus, the PVA-aided γ-Al_2O_3-coated sample displayed the best initial C.E. and cycling stability. Figure 3c further compares the rate capability of the pristine and polymer/γ-Al_2O_3-coated sample. The polymer/γ-Al_2O_3-coated NCM622 displayed 87.1% capacity retention at 5 C, much higher than 79.5% of the pristine one. Furthermore, a comparison of the Al_2O_3-coated NCM622 cathodes under a high working voltage is shown in Table S2.[15−17,30−32,34] The polymer/γ-Al_2O_3-coated NCM622 in this work displays enhanced performances on both capacity and capacity retention in long-term cycling, suggesting the superiority of the polymer-enhanced sol−gel method.

On the basis of these results, full batteries (capacity of about 2.0 mA·h) using a graphite anode were assembled and measured under high voltage of 4.5 V (Figure 3d−f), where the N/P ratio was controlled around 1.1 (Figure S3). Similar to the half batteries, the full battery using the polymer/γ-Al_2O_3-coated NCM622 cathode showed higher initial C.E. than that of the pristine one (Figure 3d). Figure 3e compares the cycling stability of the full batteries under 0.5 C (1 C = 200 mA·h g^{-1}). Remarkable highly stable cycling performance was observed for the polymer/γ-Al_2O_3-coated NCM622 sample, whose capacity remained at 154.7 mA·h g^{-1} (calculated based on the weight of the NCM622 material) after 100 cycles, corresponding to a capacity retention of 82%, whereas the pristine NCM622 sample only had a capacity of only 103.9 mA·h g^{-1} after 100 cycles and a capacity retention of 59.2%. In addition, the rate capacities of the polymer/γ-Al_2O_3-coated NCM622 sample were 6.9, 10.9, 12.4, 20.1, and 26.0% higher

DOI: 10.1021/acsomega.9b01706
ACS Omega 2019, 4, 13972−13980

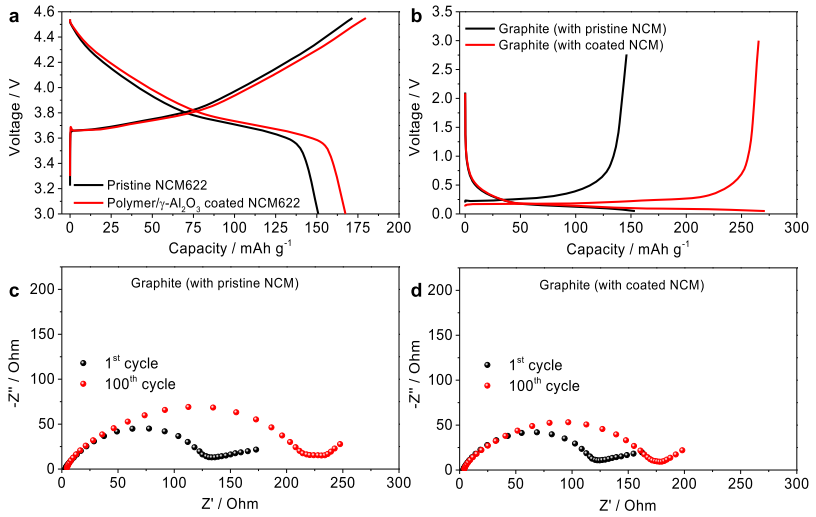

Figure 5. Remaining capacity and impedance analysis of the electrodes. Comparison of the remaining capacity of the cycled electrodes: (a) NCM622 cathodes and (b) graphite anodes. Comparison of the ac resistance of the graphite anodes cycled with the (c) pristine NCM622 cathode and (d) polymer/γ-Al_2O_3-coated NCM622 cathode at 1st and 100th cycles.

than that of the pristine one under 0.5, 1.0, 2.0, 4.0, and 5.0 C rates, respectively (Figure 3f). These results revealed a large improvement in the electrochemical performance of the polymer/γ-Al_2O_3-coated NCM622 full battery, which benefits from the continuous γ-Al_2O_3 coating on the cathode. It should be noted that in half battery measurements, the improvements of the rate discharge capacity of the polymer/γ-Al_2O_3-coated NCM622 cathode only showed 5.5, 7.0, 8.0, 7.9, and 7.3% higher than those of the pristine one under the same C-rates (Figure S4). Moreover, the capacity decay rate with an increase in the C-rate in the half-cell was also much lower than that in full battery (Figure 3b,e). These phenomena suggested that the graphite anode played a crucial role in the cycling and rate performance of the full battery, and its stability might be affected by the cathode at a high working voltage as well.

To understand the mechanism for the large improvement in the high-voltage performance of the polymer/γ-Al_2O_3-coated NCM622 sample, the area-specific impedance (ASI) of the full battery was then studied by hybrid pulse power characterization (HPPC).[35−37] The battery was first pulse discharged for 10 s at a 3 C rate, relaxed to the open-circuit voltage (OCV) for 40 s, and then finally charged for 10 s with a regenerative pulse at 75% current (2.25 C rate) of the discharge pulse (Figure S5a). The battery was fully charged and then discharged at a 1 C rate, and the discharge procedure was repeated from 10 to 90% depth of discharge (DOD), each followed by a 1 h rest period before applying the next sequence. One sequence under 20% DOD is shown in Figure S5b, in which R_{disc} was calculated via the equation: $R_{disc} = (V_0 - V_1)/i_{disc}$. The ASI and the corresponding OCV of the pristine and polymer/γ-Al_2O_3-coated NCM622 sample during cycling are shown in Figure 4a,b, respectively. It can be seen that the ASI increased much slower for the polymer/γ-Al_2O_3-coated NCM622 battery during the HPPC cycling. The largest increment of ASI appeared at 90% DOD of the battery, where the resistance increased only from 16.1 to 26.9 Ω cm^2 for the polymer/γ-Al_2O_3-coated NCM622 sample after 12 HPPC cycles, while the corresponding values of the pristine NCM622 sample increased from 17.4 Ω cm^2 to as large as 109.1 Ω cm^2. In addition, the corresponding OCVs of the polymer/γ-Al_2O_3-coated NCM622 sample under various DODs were also more stable. The electrochemical impedance spectroscopy (EIS) was also carried out to study the impedance evolution of the full battery during cycling (Figure 4c,d). The polymer/γ-Al_2O_3-coated NCM622 sample showed an R_{ct} increment of 24.7 Ω, much lower than 52.2 Ω of the pristine sample after 100 cycles. The impedance of the polymer/γ-Al_2O_3-coated NCM622 battery increased much slower than the pristine NCM622 sample, which proved that the γ-Al_2O_3 coating helped to suppress the resistance increase during cycling and led to the reduced ASI and R_{ct}.

The remaining capacities and impedances of the cathodes and anodes from the full batteries were further analyzed in detail. Two full batteries were disassembled after 100 cycling tests, and then the separated cathode and anode were reassembled into two half-cells using a lithium metal as the counter electrodes. The remaining capacity of the polymer/γ-Al_2O_3-coated and pristine NCM622 cathodes were 167.4 and 150.9 mA·h g^{-1}, corresponding to 88.7 and 88.5% of its initial capacity, respectively (Figure 5a and Table S3). The polymer/γ-Al_2O_3-coated NCM622 cathode also showed higher initial C.E. compared with the pristine one (i.e., 93.1 vs 87.9%). The R_{ct} of the polymer/γ-Al_2O_3-coated NCM622 cathode increased 8.6 Ω after 100 cycling tests, which was lower than 11.2 Ω of the pristine one (Figure S6). These results demonstrated a large decay of the NCM622 cathodes at high voltage, and polymer/γ-Al_2O_3 coating could improve its stability. However, the variation of the cathode cannot be considered as the main cause for the degradation of full battery when compared with the great value change for the corresponding graphite anode. As shown in Figure 5b, the remaining capacity of the pristine graphite anode (i.e., the anode of the full battery using a pristine NCM622 cathode after 100 cycling tests) was only 147.2 mA·h g^{-1} (0.1 C charge/discharge), corresponding to a 43.3% of its initial capacity. This could be attributed to a thick SEI formed on the electrode, leading to a high resistance (Figures 5c and S7), where R_{ct} increased 77.4 Ω. The irreversible consumption of lithium ions for the anode SEI was responsible for the quick capacity decay of the full battery.[14] However, the conditions became much better when using the polymer/γ-Al_2O_3-coated NCM622 cathode. The remaining capacity of the corresponding graphite anode could maintain as

DOI: 10.1021/acsomega.9b01706
ACS Omega 2019, 4, 13972−13980

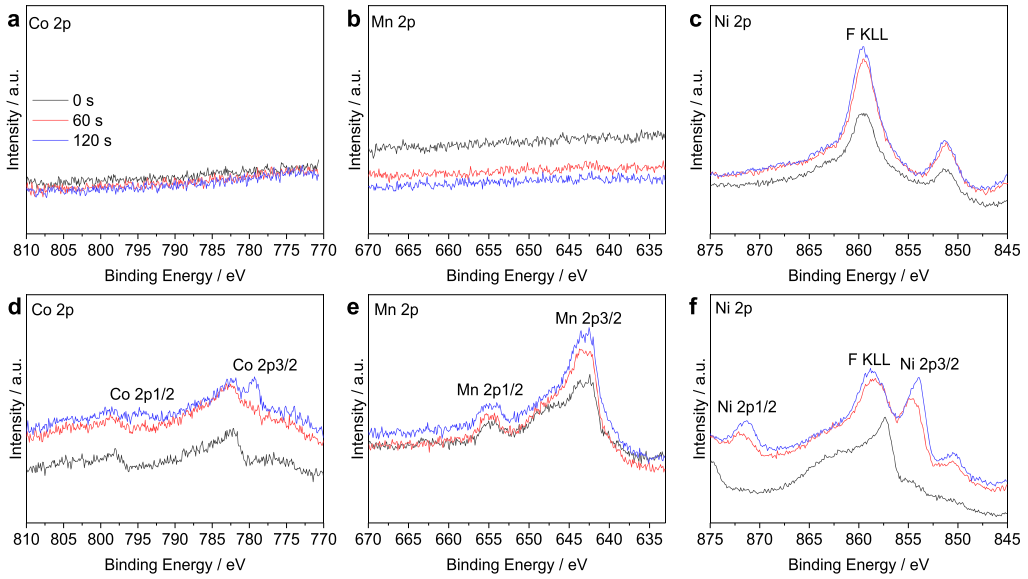

Figure 6. Surface chemistry analysis. The Ni 2p, Co 2p, and Mn 2p spectra of the graphite anodes which correspond to (a–c) polymer/γ-Al_2O_3-coated NCM622 cathode and (d–f) pristine NCM622 cathode after cycling. The etching time t = 0 s (black), 60 s (red), and 120 s (blue).

high as 265.5 mA·h g^{-1} (78.1% of its initial capacity) (Figure 5b). The R_{ct} increased only 42.3 Ω, much lower than that of the pristine graphite (Figures 5d and S7). The above results indicated that the polymer/γ-Al_2O_3 coating improved the stability of the NCM622 cathode, but more importantly, it could suppress the quick growth of SEI on the corresponding graphite anode and minimize the resistance. The reason could be that the polymer/γ-Al_2O_3 coating reduced the strong side reactions of the NCM622 cathode with the electrolyte, especially the dissolution of TMs from the cathode. The dissolved TMs could migrate from the cathode side and deposit on the surface of the graphite anode, which led to the continuous growth of the SEI and the consumption of the limited Li ions in the full battery.[14,38] Figure S8 compares the dissolution of active metal ions in the electrolyte with a vivid visualization demonstration. Two cells using a pristine cathode and polymer/γ-Al_2O_3-coated NCM62 cathode were first charged to 4.5 V and then disassembled in a glovebox. The cathodes were stored in the electrolyte (20 mg of active materials in 2 mL of electrolyte solution) at 60 °C for 2 weeks. The darker color of the pristine sample indicated that there were more TMs dissolved in the electrolyte. The ICP analysis further confirmed this result (Table S4). It was clearly shown that the dissolving amount of TMs for the polymer/γ-Al_2O_3-coated samples in the electrolyte was significantly reduced compared with the pristine sample.

The surface chemistry of the graphite anodes of the full battery after 100 cycling tests was investigated by X-ray photoelectron spectroscopy (XPS) analyses. Figure 6 shows the evolution of the Ni 2p, Mn 2p, and Co 2p spectra of the cycled graphite anodes after sputtering time t = 0, 60, and 120 s. There was no signal peak for Co 2p and Mn 2p for the coated graphite anode (i.e., the anode of the full battery using the polymer/γ-Al_2O_3-coated NCM622 cathode after 100 cycling tests) (Figure 6a,b). The reason could be that the dissolved amount of TMs was small, such that the deposition of TMs on the coated graphite anode was too low to be detected by the XPS equipment. For Ni 2p (Figure 6c), the peak at around 858 eV was obtained from the Auger electrons of the fluorine, as $LiPF_6$ decomposed during the charge–discharge process and produced LiF as SEI on the anode.[39] However, the spectra for the pristine graphite displayed quite different results, where the TM peaks appeared when the surface SEI containing F was removed after etching. The Co $2p^{3/2}$ peak at around 779.3 eV appeared after sputtering for 120 s (Figure 6d). Meanwhile, the Ni $2p^{1/2}$ (871.3 eV) and $2p^{3/2}$ (853.9 eV) signal peaks were observed after etching and became more significant with an increase in the sputtering time (Figure 6f).[40,41] These results agreed with the previous reports that the Ni and Co elements were concentrated in the inner layer of the SEI.[38,42] However, the Mn $2p^{1/2}$ and $2p^{3/2}$ peaks existed at the beginning and increased with etching (Figure 6e), indicating that the Mn element could be redissolved and deposited on the top surface of the anode SEI layers during the Li^+ deintercalation process so that the Mn element exhibited higher catalytic activity for the SEI growth.[43,44] Further XPS analysis of NCM622 cathodes after 100 cycling tests is presented in Figure S9. In contrast to the graphite anode spectra, there was not much difference between the polymer/γ-Al_2O_3-coated NCM622 and the pristine one. The spectra for Al and O elements were attached as well in Figure S10 as a reference. This observation confirmed that the control factor for the battery degradation was not the NCM622 cathode but rather the graphite anode where the deposition of TMs results in the continuous growth of the SEI and the consumption of the limited Li ions in the full battery. The polymer/γ-Al_2O_3-coated layer on the NCM622 cathode could prohibit the dissolution process effectively and remarkably enhanced battery capacity and stability under high voltage.

CONCLUSIONS

In summary, the NCM622 cathode material has been successfully coated with a thin, uniform, and microporous γ-Al_2O_3 through a PVA-aided Al_2O_3 sol–gel process. The selected polymer can facilitate the film forming while leaving micropores after sintering. The polymer/γ-Al_2O_3-coated NCM622 demonstrated significantly improved electrochemical performance when cycled at high voltage, where the cycling stability and rate capabilities were 22.8 and 26% higher than that of the pristine one, respectively. In addition, the

DOI: 10.1021/acsomega.9b01706
ACS Omega 2019, 4, 13972–13980

impedance analysis demonstrated that both DC and AC resistance of the full battery using the polymer/γ-Al_2O_3-coated NCM622 cathode remained more stable and were much lower than those of the battery using the pristine one. Battery decay mechanism analysis (i.e., remaining capacity, impedance, and surface chemistry of the cathode and anode after cycling) demonstrated that the pristine and polymer/γ-Al_2O_3-coated NCM622 cathodes exhibited a similar capacity decay, while the corresponding graphite anodes showed quite different results. The XPS analysis results further confirmed that the control factor for the battery degradation was not the decay of NCM622 cathodes but rather of the graphite anodes. This was because the dissolved TMs from the NCM622 cathode deposited on the graphite anode, leading to the continuous growth of the SEI and consumption of the limited Li ions in the full battery. The polymer/γ-Al_2O_3 coating of the NCM622 cathode has successfully suppressed the degradation through mitigating the strong side reactions, especially the dissolution of TMs.

EXPERIMENTAL SECTION

Synthesis of $LiNi_{0.6}Co_{0.2}Mn_{0.2}O_2$. $NiSO_4{\cdot}6H_2O$, $MnSO_4{\cdot}H_2O$, and $CoSO_4{\cdot}7H_2O$ (Beijing Chemical Factory, China) were first mixed, and an aqueous solution with a concentration of 2.0 mol L^{-1} MSO_4 (M = Ni, Mn, Co) was achieved. The solution was pumped into a continuously stirred tank reactor (CSTR, 2.0 L) under the N_2 atmosphere. At the same time, NaOH solution (10.0 mol L^{-1}) and $NH_3{\cdot}H_2O$ solution (10.0 mol L^{-1}, Beijing Chemical Factory, China) were fed into the CSTR separately, where the ratio of NH_3/MSO_4 was controlled strictly at 0.8. The pH value (11.00 ± 0.05), temperature (60 °C), and stirring speed (1000 rpm) were monitored and controlled carefully during the reaction process. When the coprecipitation reaction was done, the suspension was filtered, washed, and finally dried at 120 °C for 12 h. The as-obtained $Ni_{0.6}Co_{0.2}Mn_{0.2}(OH)_2$ powder was mixed thoroughly with $LiOH{\cdot}H_2O$ (Beijing Chemical Factory, China) at a molar ratio of 1:1.05. The mixture was sintered at 500 °C for 5 h and 875 °C for 12 h in the air at a rising rate of 1 °C min^{-1}. Afterward, the product was slowly cooled down to 800 °C for another 5 h and then to 500 °C under a rate of 1 °C min^{-1}.

Preparation of the γ-Al_2O_3 Sol–Gel and Surface Coating. Aluminum-tri-*sec*-butoxide [67 mL (0.25 mol), ATSB, Fluka] was added drop by drop into 170.5 mL of deionized (DI) water at 90 °C by an additional funnel. The aqueous solution was stirred for 2.5 h, while 12.5 mL of 1.0 M HNO_3 (Sigma-Aldrich) was added. Then, the solution was refluxed at 90 °C for another 12 h and cooled down. PVA (3.0 g, Fluka, MW = 72 000 g/mol) was fully dissolved in 95 mL of DI water and 5 mL of 1 M HNO_3. Then, 50 mL of PVA solution was mixed with 50 mL of the previous solution to obtain the required Al_2O_3 sol–gel. The NCM 622 active materials were washed first with DI water to remove the residue surface alkaline. Then, 50.0 g of the NCM 622 material was mixed with 20 mL of the Al_2O_3 sol–gel under stirring. After drying at 80 °C under vacuum, the powder was sintered at 550 °C for 5 h with a heating rate of 2 °C min^{-1}. For comparison, pure sol without the PVA additive was also used as a coating solution. The coating and sintering procedure was the same as above.

Material Analysis. The morphology, microstructure, and chemical composition of NCM622 cathode materials were characterized by field emission SEM (Zeiss Merlin, Germany) with EDX, TEM (FEI, Titan300 KV) equipped with high-angle annular dark-field scanning TEM , and ICP–mass spectrometry (Agilent), respectively. Powder XRD data were collected over the 2θ range 10°–80° on a Bruker D8 ADVANCE diffractometer with Cu Kα radiation (λ = 1.5406 Å, 40 kV/40 mA). The refinement of the XRD data was performed using the Fullprof software. XPS analyses were carried out on a Kratos Supra spectrometer using an Al Kα monochromatic irradiation (1486.6 eV) at a working pressure smaller than 7×10^{-8} bar. Depth profiling was carried out using Ar ion beam sputtering with 500 eV. The sputtering rate was equivalent to 0.26 nm/s on Ta_2O_5.

Electrode Preparation and Battery Assembly. The pristine or Al_2O_3-coated NCM622 powder, conductive carbon (SP and KS-6), and poly(vinylidene difluoride) (PVDF) were mixed by a weight ratio of 90:4:6 in *N*-methyl-2-pyrrolidine (NMP, Sigma-Aldrich). Graphite, super P, and PVDF were mixed with the weight ratio of 92:2:6 in NMP. These two kinds of mixtures were both mixed for 20 min using a Thinky AR-100 planetary mixer, and then the uniform slurry of NCM and graphite was cast on Al (cathode) and Cu foil (anode), respectively. The cathode and anode electrodes were dried at 120 and 90 °C, respectively, in vacuum for 6 h, and the loading density of active materials in cathode and anode electrodes was controlled around at 9.0 and 6.0 mg cm^{-2}, respectively. The battery was assembled inside the Ar-filled glovebox using a 2032-type coin cell, which consists of the NCM-622 cathode, lithium or graphite anode, Celgard 2320 separator (USA), and 1.0 M $LiPF_6$ in EC/EMC (3:7 by weight) with 2 wt % VC as the additive.

Electrochemical Measurements. The galvanostatic tests were conducted using the Neware Instrument (China) in the voltage range of 3.0–4.55 V for half batteries and 2.75–4.5 V for full batteries at room temperature. EIS measurements were completed on the electrochemical station Bio-Logic VMP3. All the batteries were measured under 50% DOD. For the EIS results of cycled graphite and NCM622 electrode, the full battery was discharged to 2.75 V after desired cycles and then disassembled in the glovebox. Then, the cycled graphite and NCM622 electrode were taken out and reassembled as a new half battery directly (without washing) using the lithium foil as the counter electrode. This type of battery aims to measure the remaining capacity and resistance of the cycled graphite and NCM622 electrode. EIS of the two half-cells was also measured at 50% DOD after one charge/discharge cycle.

HPPC was conducted during the cycling test, in which a 10 s 3.0 C discharge pulse and a 2.25 C regenerative charge pulse current were applied to the cells. There were 40 s rest periods between discharge and regenerative pulses. The pulse profiles were measured at every 10% DOD. The ASI as a function of DOD was established by calculating the voltage changes during pulses.

ASSOCIATED CONTENT

Supporting Information

The Supporting Information is available free of charge on the ACS Publications website at DOI: 10.1021/acsomega.9b01706.

Film of the polymer/γ-Al_2O_3-coated sol–gel on a glass slide and SEM top-view and cross-sectional images of the Al_2O_3 film without the PVA additive coated on the α-Al_2O_3 porous support; atomic ratio in the pristine and

DOI: 10.1021/acsomega.9b01706
ACS Omega 2019, 4, 13972–13980

polymer/γ-Al_2O_3-coated samples based on ICP-OES test; half-cell performance of first cycle capacity and Coulombic efficiency at 0.1C and cycling performance at 0.5 C for NCM622 coated with Al_2O_3 sol without the PVA additive; comparison of battery performance with Al_2O_3 coating on NCM cathode materials in half-cell; capacity match of the cathode and anode in full battery, where the N/P ratio is 1.1; rate discharge capacity comparison of the pristine and polymer/γ-Al_2O_3-coated NCM622 cathodes in half-cell and full cell; one pulse process of the HPPC test; comparison of the remaining capacity and impedance of the cycled electrodes; comparison of the ac resistance of the cycled cathodes; comparison of the SEM images of the graphite anodes from fresh, polymer/γ-Al_2O_3-coated sample battery, and pristine sample battery after 100 cycles; comparison of the dissolution of active metal ions in the electrolyte; dissolution of transition metal ions in the electrolyte for pristine and polymer/γ-Al_2O_3 NCM622 cathode; XPS spectra for Ni 2p, Co 2p, and Mn 2p for polymer/γ-Al_2O_3-coated NCM622 cathode and pristine NCM622 electrode after cycling at various sputtering times t = 0, 60, and 120; XPS spectra of Al 2p for cathodes and O 1s for all anodes and cathodes; and Raman spectra of commercial γ-Al_2O_3 powder and the coating layer sample prepared from the polymer-aided sol−gel method (PDF)

AUTHOR INFORMATION

Corresponding Authors

*E-mail: Kuo-wei.huang@kaust.edu.sa (K.-W.H.).
*E-mail: Li.yangxing@huawei.com (Y.L.).
*E-mail: Zhiping.lai@kaust.edu.sa (Z.L.).

ORCID

Thomas D. Anthopoulos: 0000-0002-0978-8813
Kuo-Wei Huang: 0000-0003-1900-2658
Zhiping Lai: 0000-0001-9555-6009

Author Contributions

Y.W. and M.L. contributed equally to this work. The manuscript was written through contributions of all authors. All authors have given approval to the final version of the manuscript.

Notes

The authors declare no competing financial interest.

ACKNOWLEDGMENTS

This work was supported by Huawei grant RGC/3/3513 and KAUST Baseline BAS/1/1375

ABBREVIATIONS

NCM, nickel cobalt manganese; PVA, polyvinyl alcohol; LIB, lithium-ion battery; TM, transition metal; SEI, solid electrolyte interface; ATSB, aluminum-tri-*sec*-butoxide; EIS, electrochemical impedance spectroscopy; DOD, depth of discharge; HPPC, hybrid pulse power characterization; C.E., Coulombic efficiency; ASI, area-specific impedance; OCV, open-circuit voltage

REFERENCES

(1) Schipper, F.; Erickson, E. M.; Erk, C.; Shin, J.-Y.; Chesneau, F. F.; Aurbach, D. Recent advances and remaining challenges for lithium ion battery cathodes I. Nickel-Rich, $LiNi_xCo_yMnzO_2$. *J. Electrochem. Soc.* **2017**, *164*, A6220−A6228.

(2) Li, W.; Song, B.; Manthiram, A. High-voltage positive electrode materials for lithium-ion batteries. *Chem. Soc. Rev.* **2017**, *46*, 3006−3059.

(3) Nitta, N.; Wu, F.; Lee, J. T.; Yushin, G. Li-ion battery materials: present and future. *Mater. Today* **2015**, *18*, 252−264.

(4) Shi, J. L.; Xiao, D. D.; Ge, M. Y.; Yu, X. Q.; Chu, Y.; Huang, X. J.; Zhang, X. D.; Yin, Y. X.; Yang, X. Q.; Guo, Y. G.; Gu, L.; Wan, L. J. High-Capacity Cathode Material with High Voltage for Li-Ion Batteries. *Adv. Mater.* **2018**, *30* (). DOI: 10.1002/adma.201705575

(5) Noh, H.-J.; Youn, S.; Yoon, C. S.; Sun, Y.-K. Comparison of the structural and electrochemical properties of layered $Li[Ni_xCo_yMn_z]O_2$ (x = 1/3, 0.5, 0.6, 0.7, 0.8 and 0.85) cathode material for lithium-ion batteries. *J. Power Sources* **2013**, *233*, 121−130.

(6) Kim, J.; Lee, H.; Cha, H.; Yoon, M.; Park, M.; Cho, J. Prospect and Reality of Ni-Rich Cathode for Commercialization. *Adv. Energy Mater.* **2018**, *8*, 1702028.

(7) Yan, P.; Zheng, J.; Liu, J.; Wang, B.; Cheng, X.; Zhang, Y.; Sun, X.; Wang, C.; Zhang, J.-G. Tailoring grain boundary structures and chemistry of Ni-rich layered cathodes for enhanced cycle stability of lithium-ion batteries. *Nat. Energy* **2018**, *3*, 600−605.

(8) Zhang, H.; Omenya, F.; Yan, P.; Luo, L.; Whittingham, M. S.; Wang, C.; Zhou, G. Rock-Salt Growth-Induced (003) Cracking in a Layered Positive Electrode for Li-Ion Batteries. *ACS Energy Lett* **2017**, *2*, 2607−2615.

(9) Nam, K.-W.; Bak, S.-M.; Hu, E.; Yu, X.; Zhou, Y.; Wang, X.; Wu, L.; Zhu, Y.; Chung, K.-Y.; Yang, X.-Q. Combining in situ synchrotron X-ray diffraction and absorption techniques with transmission electron microscopy to study the origin of thermal instability in overcharged cathode materials for lithium-ion batteries. *Adv. Funct. Mater.* **2013**, *23*, 1047−1063.

(10) Chen, Z.; Chao, D.; Lin, J.; Shen, Z. Recent progress in surface coating of layered $LiNi_xCo_yMn_zO_2$ for lithium-ion batteries. *Mater. Res. Bull.* **2017**, *96*, 491−502.

(11) Jung, S.-K.; Gwon, H.; Hong, J.; Park, K.-Y.; Seo, D.-H.; Kim, H.; Hyun, J.; Yang, W.; Kang, K. Understanding the Degradation Mechanisms of $LiNi_{0.5}Co_{0.2}Mn_{0.3}O_2$ Cathode Material in Lithium Ion Batteries. *Adv. Energy Mater.* **2014**, *4*, 1300787.

(12) Zheng, J.; Gu, M.; Xiao, J.; Zuo, P.; Wang, C.; Zhang, J.-G. Corrosion/fragmentation of layered composite cathode and related capacity/voltage fading during cycling process. *Nano Lett.* **2013**, *13*, 3824−3830.

(13) Stiaszny, B.; Ziegler, J. C.; Krauß, E. E.; Zhang, M.; Schmidt, J. P.; Ivers-Tiffée, E. Electrochemical characterization and post-mortem analysis of aged $LiMn_2O_4$−NMC/graphite lithium ion batteries part II: Calendar aging. *J. Power Sources* **2014**, *258*, 61−75.

(14) Li, D.; Li, H.; Danilov, D. L.; Gao, L.; Chen, X.; Zhang, Z.; Zhou, J.; Eichel, R.-A.; Yang, Y.; Notten, P. H. L. Degradation mechanisms of $C_6/LiNi_{0.5}Mn_{0.3}Co_{0.2}O_2$ Li-ion batteries unraveled by non-destructive and post-mortem methods. *J. Power Sources* **2019**, *416*, 163−174.

(15) Liu, W.; Li, X.; Xiong, D.; Hao, Y.; Li, J.; Kou, H.; Yan, B.; Li, D.; Lu, S.; Koo, A.; Adair, K.; Sun, X. Significantly improving cycling performance of cathodes in lithium ion batteries: The effect of Al_2O_3 and $LiAlO_2$ coatings on $LiNi_{0.6}Co_{0.2}Mn_{0.2}O_2$. *Nano Energy* **2018**, *44*, 111−120.

(16) Wang, J.; Du, C.; Yan, C.; He, X.; Song, B.; Yin, G.; Zuo, P.; Cheng, X. Al_2O_3 coated concentration-gradient $Li[Ni_{0.73}Co_{0.12}Mn_{0.15}]O_2$ cathode material by freeze drying for long-life lithium ion batteries. *Electrochim. Acta* **2015**, *174*, 1185−1191.

(17) Lee, Y.-S.; Shin, W.-K.; Kannan, A. G.; Koo, S. M.; Kim, D.-W. Improvement of the Cycling Performance and Thermal Stability of Lithium-Ion Cells by Double-Layer Coating of Cathode Materials with Al_2O_3 Nanoparticles and Conductive Polymer. *ACS Appl. Mater. Interfaces* **2015**, *7*, 13944−13951.

(18) Chen, Y.; Zhang, Y.; Chen, B.; Wang, Z.; Lu, C. An approach to application for $LiNi_{0.6}Co_{0.2}Mn_{0.2}O_2$ cathode material at high cutoff voltage by TiO_2 coating. *J. Power Sources* **2014**, *256*, 20−27.

DOI: 10.1021/acsomega.9b01706
ACS Omega 2019, 4, 13972−13980

(19) Wu, F.; Wang, M.; Su, Y.; Chen, S.; Xu, B. Effect of TiO_2-coating on the electrochemical performances of $LiCo_{1/3}Ni_{1/3}Mn_{1/3}O_2$. *J. Power Sources* **2009**, *191*, 628−632.
(20) Cho, Y.; Lee, Y.-S.; Park, S.-A.; Lee, Y.; Cho, J. $LiNi_{0.8}Co_{0.15}Al_{0.05}O_2$ cathode materials prepared by TiO_2 nanoparticle coatings on $Ni_{0.8}Co_{0.15}Al_{0.05}(OH)_2$ Precursors. *Electrochim. Acta* **2010**, *56*, 333−339.
(21) Chen, Z.; Dahn, J. R. Effect of a ZrO_2 coating on the structure and electrochemistry of Li_xCoO_2 when cycled to 4.5 V. *Electrochem. Solid State Lett.* **2002**, *5*, A213−A216.
(22) Hu, S.-K.; Cheng, G.-H.; Cheng, M.-Y.; Hwang, B.-J.; Santhanam, R. Cycle life improvement of ZrO_2-coated spherical $LiNi_{1/3}Co_{1/3}Mn_{1/3}O_2$ cathode material for lithium ion batteries. *J. Power Sources* **2009**, *188*, 564−569.
(23) Lee, S. M.; Oh, S. H.; Ahn, J. P.; Cho, W. I.; Jang, H. Electrochemical properties of ZrO_2-coated $LiNi_{0.8}Co_{0.2}O_2$ cathode materials. *J. Power Sources* **2006**, *159*, 1334−1339.
(24) Cho, J.; Kim, T.-J.; Kim, J.; Noh, M.; Park, B. Synthesis, thermal, and electrochemical properties of $AlPO_4$-coated $Li-Ni_{0.8}Co_{0.1}Mn_{0.1}O_2$ cathode materials for a Li-ion cell. *J. Electrochem. Soc.* **2004**, *151*, A1899−A1904.
(25) Tan, K.; Reddy, M.; Rao, G.; Chowdari, B. Effect of $AlPO_4$-coating on cathodic behaviour of $Li(Ni_{0.8}Co_{0.2})O_2$. *J. Power Sources* **2005**, *141*, 129−142.
(26) Wu, Y.; Ming, H.; Li, M.; Zhang, J.; Wahyudi, W.; Xie, L.; He, X.; Wang, J.; Wu, Y.; Ming, J. New Organic Complex for Lithium Layered Oxide Modification: Ultrathin Coating, High-Voltage, and Safety Performances. *ACS Energy Lett* **2019**, *4*, 656−665.
(27) Sun, Y.-K.; Cho, S.-W.; Lee, S.-W.; Yoon, C. S.; Amine, K. AlF_3-coating to improve high voltage cycling performance of $Li-[Ni_{1/3}Co_{1/3}Mn_{1/3}]O_2$ cathode materials for lithium secondary batteries. *J. Electrochem. Soc.* **2007**, *154*, A168−A172.
(28) Lee, S.-H.; Yoon, C. S.; Amine, K.; Sun, Y.-K. Improvement of long-term cycling performance of $Li[Ni_{0.8}Co_{0.15}Al_{0.05}]O_2$ by AlF_3 coating. *J. Power Sources* **2013**, *234*, 201−207.
(29) Park, B.-C.; Kim, H.-B.; Myung, S.-T.; Amine, K.; Belharouak, I.; Lee, S.-M.; Sun, Y.-K. Improvement of structural and electrochemical properties of AlF_3-coated $Li[Ni_{1/3}Co_{1/3}Mn_{1/3}]O_2$ cathode materials on high voltage region. *J. Power Sources* **2008**, *178*, 826−831.
(30) Shi, Y.; Zhang, M.; Qian, D.; Meng, Y. S. Ultrathin Al_2O_3 Coatings for Improved Cycling Performance and Thermal Stability of $LiNi_{0.5}Co_{0.2}Mn_{0.3}O_2$ Cathode Material. *Electrochim. Acta* **2016**, *203*, 154−161.
(31) Su, Y.; Cui, S.; Zhuo, Z.; Yang, W.; Wang, X.; Pan, F. Enhancing the High-Voltage Cycling Performance of $Li-Ni_{0.5}Mn_{0.3}Co_{0.2}O_2$ by Retarding Its Interfacial Reaction with an Electrolyte by Atomic-Layer-Deposited Al_2O_3. *ACS Appl. Mater. Interfaces* **2015**, *7*, 25105−25112.
(32) Wise, A. M.; Ban, C.; Weker, J. N.; Misra, S.; Cavanagh, A. S.; Wu, Z.; Li, Z.; Whittingham, M. S.; Xu, K.; George, S. M.; Toney, M. F. Effect of Al_2O_3 Coating on Stabilizing $LiNi_{0.4}Mn_{0.4}Co_{0.2}O_2$ Cathodes. *Chem. Mater.* **2015**, *27*, 6146−6154.
(33) Xie, J.; Zhao, J.; Liu, Y.; Wang, H.; Liu, C.; Wu, T.; Hsu, P.-C.; Lin, D.; Jin, Y.; Cui, Y. Engineering the surface of $LiCoO_2$ electrodes using atomic layer deposition for stable high-voltage lithium ion batteries. *Nano Res.* **2017**, *10*, 3754−3764.
(34) Chen, Y.; Zhang, Y.; Wang, F.; Wang, Z.; Zhang, Q. Improve the structure and electrochemical performance of $LiNi_{0.6}Co_{0.2}Mn_{0.2}O_2$ cathode material by nano-Al_2O_3 ultrasonic coating. *J. Alloys Compd.* **2014**, *611*, 135−141.
(35) Liu, Q.; Su, X.; Lei, D.; Qin, Y.; Wen, J.; Guo, F.; Wu, Y. A.; Rong, Y.; Kou, R.; Xiao, X.; Aguesse, F.; Bareño, J.; Ren, Y.; Lu, W.; Li, Y. Approaching the capacity limit of lithium cobalt oxide in lithium ion batteries via lanthanum and aluminium doping. *Nat. Energy* **2018**, *3*, 936−943.
(36) Solchenbach, S.; Hong, G.; Freiberg, A. T. S.; Jung, R.; Gasteiger, H. A. Electrolyte and SEI Decomposition Reactions of Transition Metal Ions Investigated by On-Line Electrochemical Mass Spectrometry. *J. Electrochem. Soc.* **2018**, *165*, A3304−A3312.
(37) Beninati, S.; Damen, L.; Mastragostino, M. Fast sol-gel synthesis of $LiFePO_4/C$ for high power lithium-ion batteries for hybrid electric vehicle application. *J. Power Sources* **2009**, *194*, 1094−1098.
(38) Li, D.; Li, H.; Danilov, D.; Gao, L.; Zhou, J.; Eichel, R.-A.; Yang, Y.; Notten, P. H. L. Temperature-dependent cycling performance and ageing mechanisms of $C_6/LiNi_{1/3}Mn_{1/3}Co_{1/3}O_2$ batteries. *J. Power Sources* **2018**, *396*, 444−452.
(39) Militello, M. C.; Gaarenstroom, S. W. Graphite-Filled Poly (vinylidene fluoride) (PVDF) by XPS. *Surf. Sci. Spectra* **1999**, *6*, 141−145.
(40) Li, D.; Danilov, D.; Zhang, Z.; Chen, H.; Yang, Y.; Notten, P. H. L. Modeling the SEI-Formation on Graphite Electrodes in $LiFePO_4$ Batteries. *J. Electrochem. Soc.* **2015**, *162*, A858−A869.
(41) Grosvenor, A. P.; Biesinger, M. C.; Smart, R. S. C.; McIntyre, N. S. New interpretations of XPS spectra of nickel metal and oxides. *Surf. Sci.* **2006**, *600*, 1771−1779.
(42) Jung, R.; Linsenmann, F.; Thomas, R.; Wandt, J.; Solchenbach, S.; Maglia, F.; Stinner, C.; Tromp, M.; Gasteiger, H. A. Nickel, Manganese, and Cobalt Dissolution from Ni-Rich NMC and Their Effects on NMC622-Graphite Cell. *J. Electrochem. Soc.* **2019**, *166*, A378−A389.
(43) Xiao, X.; Liu, Z.; Baggetto, L.; Veith, G. M.; More, K. L.; Unocic, R. R. Unraveling manganese dissolution/deposition mechanisms on the negative electrode in lithium ion batteries. *Phys. Chem. Chem. Phys.* **2014**, *16*, 10398−10402.
(44) Gowda, S. R.; Gallagher, K. G.; Croy, J. R.; Bettge, M.; Thackeray, M. M.; Balasubramanian, M. Oxidation state of cross-over manganese species on the graphite electrode of lithium-ion cells. *Phys. Chem. Chem. Phys.* **2014**, *16*, 6898−6902.

DOI: 10.1021/acsomega.9b01706
ACS Omega 2019, 4, 13972−13980